



Reentrant excitation in an analog-digital hybrid circuit model of cardiac tissue

Farhanahani Mahmud, Naruhiro Shiozawa, Masaaki Makikawa, and Taishin Nomura

Citation: [Chaos 21, 023121 \(2011\)](#); doi: [10.1063/1.3597645](https://doi.org/10.1063/1.3597645)

View online: <http://dx.doi.org/10.1063/1.3597645>

View Table of Contents: <http://scitation.aip.org/content/aip/journal/chaos/21/2?ver=pdfcov>

Published by the [AIP Publishing](#)

Articles you may be interested in

[Unstable spiral waves and local Euclidean symmetry in a model of cardiac tissue](#)

Chaos **25**, 063116 (2015); [10.1063/1.4922596](https://doi.org/10.1063/1.4922596)

[Continuous-waveform constant-current isolated physiological stimulator](#)

Rev. Sci. Instrum. **83**, 044303 (2012); [10.1063/1.3700977](https://doi.org/10.1063/1.3700977)

[The role of M cells and the long QT syndrome in cardiac arrhythmias: Simulation studies of reentrant excitations using a detailed electrophysiological model](#)

Chaos **14**, 172 (2004); [10.1063/1.1636272](https://doi.org/10.1063/1.1636272)

[A numerical method for the solution of the bidomain equations in cardiac tissue](#)

Chaos **8**, 234 (1998); [10.1063/1.166300](https://doi.org/10.1063/1.166300)

[Models of defibrillation of cardiac tissue](#)

Chaos **8**, 188 (1998); [10.1063/1.166297](https://doi.org/10.1063/1.166297)

The image shows several copies of the journal "Computing in Science & Engineering" displayed on a shelf. The cover of the journal features a colorful graphic of a hurricane and the title "HURRICANE PREDICTOR". At the bottom of the image, there is a large, bold text overlay that reads "AIP's JOURNAL OF COMPUTATIONAL TOOLS AND METHODS. AVAILABLE AT MOST LIBRARIES." The "Computing" logo is also present in the bottom right corner.

Reentrant excitation in an analog-digital hybrid circuit model of cardiac tissue

Farhanahani Mahmud,¹ Naruhiro Shiozawa,² Masaaki Makikawa,³ and Taishin Nomura¹

¹Graduate School of Engineering Science, Osaka University, Osaka 5608534, Japan

²College of Sport and Health Science, Ritsumeikan University, Kusatsu, Shiga, Japan

³College of Science and Engineering, Ritsumeikan University, Kusatsu, Shiga, Japan

(Received 7 December 2010; accepted 16 May 2011; published online 21 June 2011)

We propose an analog-digital hybrid circuit model of one-dimensional cardiac tissue with hardware implementation that allows us to perform real-time simulations of spatially conducting cardiac action potentials. Each active nodal compartment of the tissue model is designed using analog circuits and a dsPIC microcontroller, by which the time-dependent and time-independent nonlinear current-voltage relationships of six types of ion channel currents employed in the Luo-Rudy phase I (LR-I) model for a single mammalian cardiac ventricular cell can be reproduced quantitatively. Here, we perform real-time simulations of reentrant excitation conduction in a ring-shaped tissue model that includes eighty nodal compartments. In particular, we show that the hybrid tissue model can exhibit real-time dynamics for initiation of reentries induced by unidirectional block, as well as those for phase resetting that leads to annihilation of the reentry in response to impulsive current stimulations at appropriate nodes and timings. The dynamics of the hybrid model are comparable to those of a spatially distributed tissue model with LR-I compartments. Thus, it is conceivable that the hybrid model might be a useful tool for large scale simulations of cardiac tissue dynamics, as an alternative to numerical simulations, leading toward further understanding of the reentrant mechanisms. © 2011 American Institute of Physics. [doi:10.1063/1.3597645]

Dysfunction of electrical excitations and their spatial propagation in cardiac myocytes can induce abnormal contractions of the heart, leading to life threatening arrhythmias. Some arrhythmias are perpetuated by reentrant mechanisms, in which a local excitation conducts through a part of the heart to recirculate back to the original site. This reentry cycle time can be shorter than the normal cycle of a cardiac pacemaker, leading to the rapid heart beat referred to as a reentrant tachycardia. To better understand electrophysiological mechanisms of the reentrant arrhythmias at the cellular, tissue, and organ levels, mathematical models of cardiac cells, tissues, and the heart have been developed in order to simulate the propagation of excitations in a variety of conditions. However, it is inevitable for those models to become large scale in the number of dynamical variables, requiring immense amounts of computational time for their dynamic simulations. Here, we introduce an analog-digital hybrid circuit model of electrical excitation of a cardiac cell based on the Luo-Rudy phase I model, a typical mathematical model for a cardiac cell. The hybrid circuit model, through its hardware-implementation, allows us to perform real-time simulation of cellular excitations as well as their propagation in a network of hybrid cell models as a cardiac tissue model. The hardware-implemented tissue model inherits the real-time capability of the single hybrid cell model, independent of the size of the tissue network. To our best knowledge, this is the first attempt to design and

implement a hardware circuit model of spatially distributed cardiac tissue with biophysically detailed ion channel currents responsible for cellular excitations.

I. INTRODUCTION

Contraction of a cardiac myocyte is triggered by a membrane action potential, which is controlled by transmembrane currents through various types of ion channels.^{1,2} Major ion currents include the fast inward Na^+ current, the transient outward K^+ current, the slow inward Ca^{2+} current, the slow delayed rectifier K^+ current, and the slow delayed rectifier K^+ outward current, among others. A cardiac action potential, referred to also as excitation, is often generated in response to a supra-threshold current stimulation. The excitability of the cell decreases for a period of time after a prior excitation, causing the refractoriness of the cell. The heart consists of a huge number of such excitable cells,³ about 20 million myocytes in adult rats⁴ and about 800 million myocytes in human ventricles,⁵ connected locally by the gap junctions that allow spatial conductions of action potentials through the heart tissue. Thus, the heart is a typical large scale excitable medium that can potentially exhibit reentry excitations such as spiral waves of conducting excitations.^{6–11} Some cardiac arrhythmias are perpetuated by reentrant mechanisms, in which a local excitation conducts through a part of the heart to

recirculate back to the original site, causing a rapid heart beat referred to as reentrant tachycardia.¹²

Methodologies that have been employed so far to theoretically understand the nonlinear dynamics of excitable media include mathematical modelings with computer simulations as well as electronic experiments that utilize hardware-implemented nonlinear circuits, by which experimentally observed dynamics of real-world excitable media have been reproduced and analyzed qualitatively and/or quantitatively. The use of mathematical models with computer simulations is favorable because of their large capability for describing physical and/or physiological mechanisms in detail, allowing practically one-to-one correspondence between parameters in the models and real physical quantities. Indeed, mathematical models of the ventricular cardiac action potential in single cells have continued their remarkable development and improvement after the Hodgkin-Huxley formulation¹³ with the gating theory of conductance-based ion channel dynamics, initiated in the first modeling attempt by FitzHugh¹⁴ and Noble,¹⁵ continued by Beeler and Reuter,¹⁶ Luo and Rudy,^{17–19} and many others including models with Markov-type channel kinetics,² until today as described in Refs. 2 and 20–22. A large number of detailed physical state variables have been introduced in recent models in order to take new experimental observations at the cellular, sub-cellular, and molecular levels into account.^{22–25} Therefore, some of the recent studies at the tissue and organ levels try to use such detailed biophysical models to investigate excitation conductions in heart tissue.^{26–31} However, tissue models, as well as whole ventricle models, should consist of a large number of single cell models, which causes a new problem in the amount of computations required to obtain meaningful steady-state dynamics from their simulations.^{32,33} Due to this drawback, it is a still challenging issue to simulate dynamics of cardiac tissue models consisting of the latest detailed single cell models as their compartmental nodes. In this respect, it is also important to develop minimal models that can quantitatively reproduce the variety aspects of dynamic characteristics, such as restitution curves, of detailed biophysical models and use them for tissue level simulations.^{34,35}

Hardware-implemented excitable media have their own long history of investigation, comparable to that of the mathematical models, as traced back to circuits of excitable systems proposed in the 1960s (Refs. 36–38). In particular, Nagumo *et al.*³⁷ demonstrated that their active transmission line involving nine active nodal compartments could simulate propagating action potentials along a nerve axon, in which each active node was implemented by a tunnel diode with an N-shaped current-voltage (*I*-*V*) relationship mimicking the one in the Bonhoeffer-van der Pol model.³⁹ Advantages to developing hardware-implemented excitable media include their capability for performing real-time computations of their dynamics, independent of the size of the system, i.e., the number of excitable nodal compartments used in the systems, as well as their potential use in medical engineering applications. Although fewer attempts⁴⁰ have been made for hardware implementation of spatially distributed excitable media after Nagumo *et al.*, developments of circuit models mimicking neuronal and cardiac cellular dynamics have been continued. Hoshimiya *et al.*⁴¹ proposed an electronic circuit model of

excitable membrane realized by a single time-dependent (transient) *I*-*V* relationship determining a total membrane current through different types of ion channels. Maeda *et al.*^{42,43} and Sekine *et al.*^{44,45} constructed analog circuit models with two or three ion channel currents in which *I*-*V* relationships were activated at different time scales in order to simulate bursting or pacemaker type neuronal excitations. These circuit models are beneficial for studying the nonlinear dynamics of excitable media qualitatively. However, due to the qualitative design of their *I*-*V* relationships, it is usually difficult to establish explicit correspondence between the currents in a hardware circuit model and the ion channel currents of an excitable cell unlike in the case of the mathematical models. Only a few studies have succeeded to design analog circuits that are biophysically detailed and have quantitative correspondence to a real cell.⁴⁶

One of the main issues for studying excitation conductions in the field of cardiac physiology and pathology is understanding how the action potential conduction and reentry dynamics at the tissue level are influenced by cellular level dysfunction of specific ion channels^{28,47–49} that cause abnormal cellular excitation such as in long QT syndrome.⁵⁰ In order to provide comprehensive answers to this sort of question using a mathematical or hardware circuit model of cardiac tissue, it is required for every cellular model (compartmental node) used in the tissue model to include physiologically and quantitatively plausible models of ion channel currents rather than simple and qualitative models.

Recently, we have proposed a hardware circuit model of an excitable cell that can quantitatively reproduce the action potential generation and phase-locked and chaotic responses to periodic current pulse stimulations observed in the Luo-Rudy phase I (LR-I) model¹⁷ for a mammalian cardiac ventricular cell based on comparisons in the action potential waveforms and bifurcation diagrams that shows parameter regions for various phase-locked dynamics.⁵¹ Here, we first report a slightly modified version of the circuit model briefly. We then propose a model of a spatially distributed extension of a one-dimensional cardiac tissue with its hardware implementation. The circuit model allows us to perform real-time simulations of spatially conducting cardiac action potentials. In particular, we show that the circuit tissue model can exhibit real-time dynamics for initiation of the reentry induced by uni-directional block and for phase resetting that leads to annihilation of the reentry in response to impulsive current stimulations at appropriate locations and timings. The dynamics of the hybrid model are compared to those obtained numerically by the LR-I model in order to demonstrate that the circuit model can be utilized for simulating large scale cellular network in real-time as an alternative to numerical simulations.

II. BRIEF SUMMARY OF LUO-RUDY I MODEL AND ANALOG-DIGITAL HYBRID ACTIVE CIRCUIT OF A CARDIAC CELL

A. Luo-Rudy I model

The LR-I model is described by a set of nonlinear ordinary differential equations that includes eight dynamic state

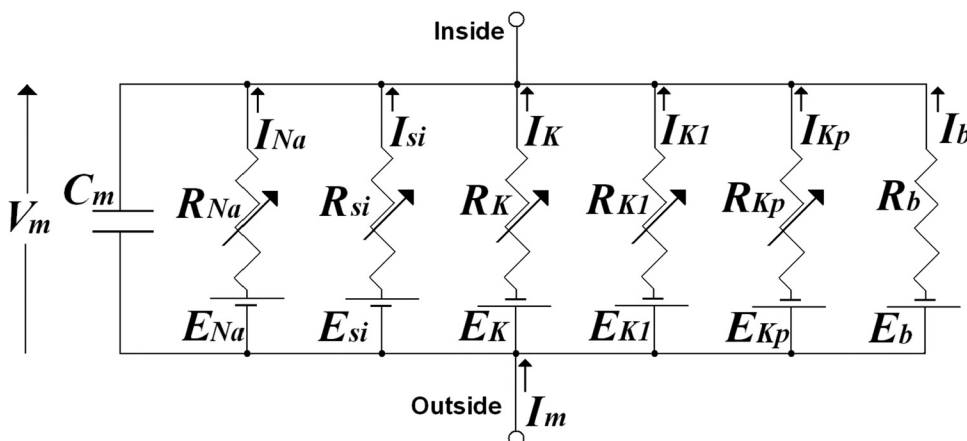


FIG. 1. An equivalent circuit of LR-I model.

variables with six types of ion channel currents. The ion channel currents are the fast inward sodium current I_{Na} , the slow inward current I_{si} carried mainly by calcium ions, the time-dependent potassium current I_K , the time-independent potassium current I_{K1} , the time-independent plateau potassium current I_{Kp} , and the background current I_b carried by sodium, potassium, and calcium ions. See Fig. 1 for an equivalent electrical circuit where V_m is the membrane potential. The voltage source in each channel represents the electro-chemical Nernst potential of the corresponding ion. The six ion channel currents are summed to give the total channel current I_{ion} as in Eq. (1). Placing I_{ion} in parallel to the current through the capacitive component of the membrane circuit C_m yields Eq. (2) for the total current flow I_m through the membrane,

$$I_{ion} = I_{Na} + I_{si} + I_K + I_{K1} + I_{Kp} + I_b, \quad (1)$$

$$I_m = C_m \frac{dV_m}{dt} + I_{ion}. \quad (2)$$

Note that the membrane current I_m corresponds to, and is always equal to, stimulation current applied externally to the membrane.

B. Hybrid cell model

The analog-digital hybrid active circuit for a single cardiac cell, referred to here as the hybrid cell model, includes analog circuits and the digital circuit of a dsPIC microcontroller. The core part of the hybrid cell model was designed as shown in Fig. 2. Four out of the six ion channel branches were designed using analog circuits, and the remaining two branches were lumped together using the single dsPIC. The action potentials of the hybrid cell model were produced by injecting external current stimulations, I_{ext} , which should be equal to I_m in Eq. (2). A validation criterion for each of the six branches in the hybrid cell model to be quantitatively close to the corresponding ion channel in LR-I model was set if the transient and/or steady-state nonlinear $I-V$ relationships of the ion channel in LR-I could be reproduced quantitatively by the circuit branch in the hybrid cell model. The analog circuits were used to implement the time-independent ion currents of I_{K1} , I_{Kp} , and I_b , and the time-dependent fast sodium current I_{Na} which has a rela-

tively short time constant. We designed each of these analog circuits by exploiting the intrinsic voltage-current relationships of bipolar transistors (Tr), resistors (R), capacitors (C), and voltage sources to reproduce the steady-state $I-V$ relationships for I_{K1} , I_{Kp} , and I_b , and the transient as well as the steady-state $I-V$ relationships for I_{Na} . An electronic circuit simulation tool (Altium Designer version 6, Australia) was utilized to design these analog circuits. I_K and I_{si} were reproduced by the digital part of the hybrid cell model using a 16-bit high-performance dsPIC30f4011 microcontroller (Microchip Technology, USA) with a processing speed of 120 MHz. To increase the speed of calculation, we accessed certain data from pre-constructed lookup tables stored in the memory (ROM) rather than calculating the functions in equations which represent the ion channel currents. In particular, seven nonlinear static functions (α_d , β_d , α_f , β_f , α_X , β_X , and X_i) of the membrane potential V_m were stored as tables in ROM for a range of V_m between -100 and 120 mV with a resolution (step) of 0.5 mV. For V_m values between the resolution step of the table, the nearest value of the table was used as an output of each function. See supplemental material⁶⁶ for details.

Figure 3 illustrates the overall circuit of the hybrid cell model with its marginal circuits, where the core part is depicted as two boxes denoted as the digital and analog parts. Detailed circuit diagrams of the analog and digital parts of the core circuit are shown separately in Figs. 4 and 5, respectively. The circuit branches of (a), (b), (c), and (d) in

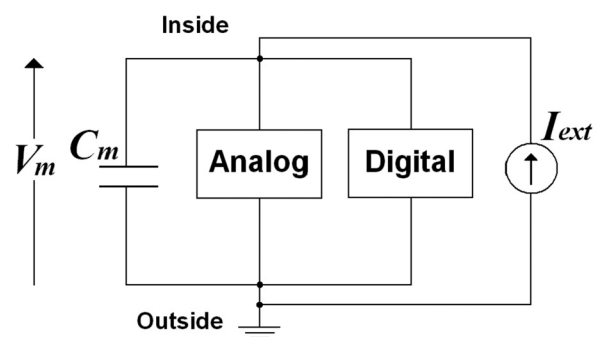


FIG. 2. The analog-digital hybrid cell model. Ion channel currents are implemented by analog and digital circuits that are placed in parallel with C_m representing the membrane capacitance.

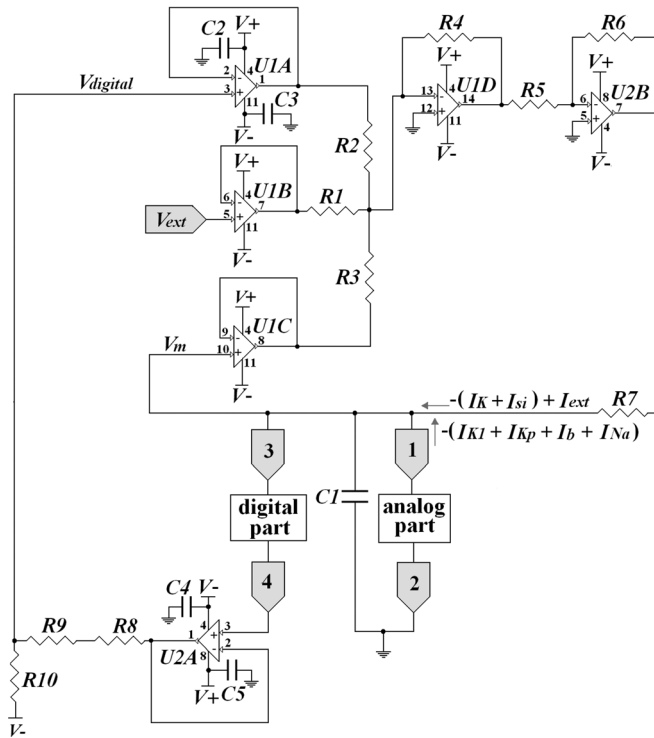


FIG. 3. The overall circuit diagram of the analog-digital hybrid cell model.

Fig. 4 represent I_{K1} , I_{Kp} , I_b , and I_{Na} , respectively. The overall hybrid cell model is powered by the direct current (dc) power supplies of 9 (V+) and -9 V (V-) as shown in Fig. 3. Circuit diagrams necessary for providing the voltage sources (V_1 to V_9) in the analog part of Fig. 4 and a power circuit for generating V_{CC} (5 V) in the digital part of Fig. 5 are shown in the Appendix. Details of all electronic components used to construct

the analog-digital cell model and the source program executed by the dsPIC are provided as supplemental material.⁶⁶

Let us illustrate how the hybrid cell model behaves by referring to Fig. 3. We start with a voltage signal at the terminal 1 of Fig. 3, which is identical with the terminal 1 of Fig. 4, corresponding to the cardiac cell membrane potential V_m . This V_m is fed into the port of a 10-bit analog to digital converter of the dsPIC at terminal 3 of Fig. 3, sampled with a frequency of 2.5 kHz. I_K and I_{si} are then computed in the dsPIC at each instant of time for a given V_m to generate the output voltage from the digital part at the terminal 4 of Fig. 3 through a 10-bit digital to analog converter. This output voltage is proportional to the sum of I_K and I_{si} , determining the value of $V_{digital}$ that is fed-back into the analog circuit. The amount of externally injected pulsatile stimulus current I_{ext} is given by a command voltage pulse V_{ext} . The voltages $V_{digital}$, V_{ext} , and the membrane potential V_m are summed up to generate the potential difference between $V_{digital} + V_{ext} + V_m$ and V_m as $V_{digital} + V_{ext}$ which induces the current $-I_K - I_{si} + I_{ext}$ by using the resistor R_7 . Kirchhoff's laws applied at the T-shaped branch at the upper part of the capacitance C_1 of Fig. 3 ensure that the sum of $-I_K - I_{si} + I_{ext}$, $-I_{Na} - I_{K1} - I_{Kp} - I_b$, and $-C_1 dV_m/dt$ is equal to zero. That is, the equality

$$-C_1 \frac{dV_m}{dt} - I_{ion} + I_{ext} = 0, \quad (3)$$

holds as in Eq. (2).

The time scale of the analog-digital hybrid cell model was set to be the same as that of LR-I model. The current and voltage scales of the analog-digital hybrid cell model (milli-ampere and volt) were not the same as those of the LR-I model (micro-ampere and milli-volt). The scale conversions of the voltage and the current were performed because

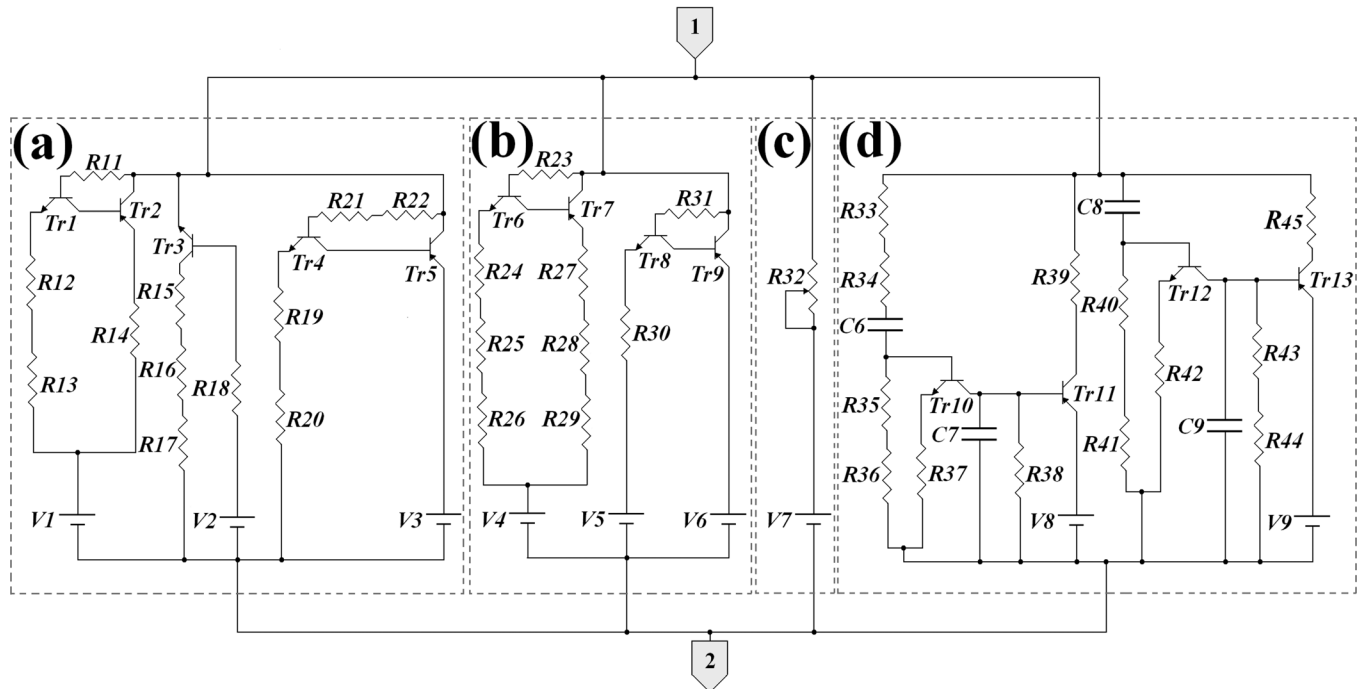


FIG. 4. The circuit diagram of the analog part in the analog-digital hybrid cell model.

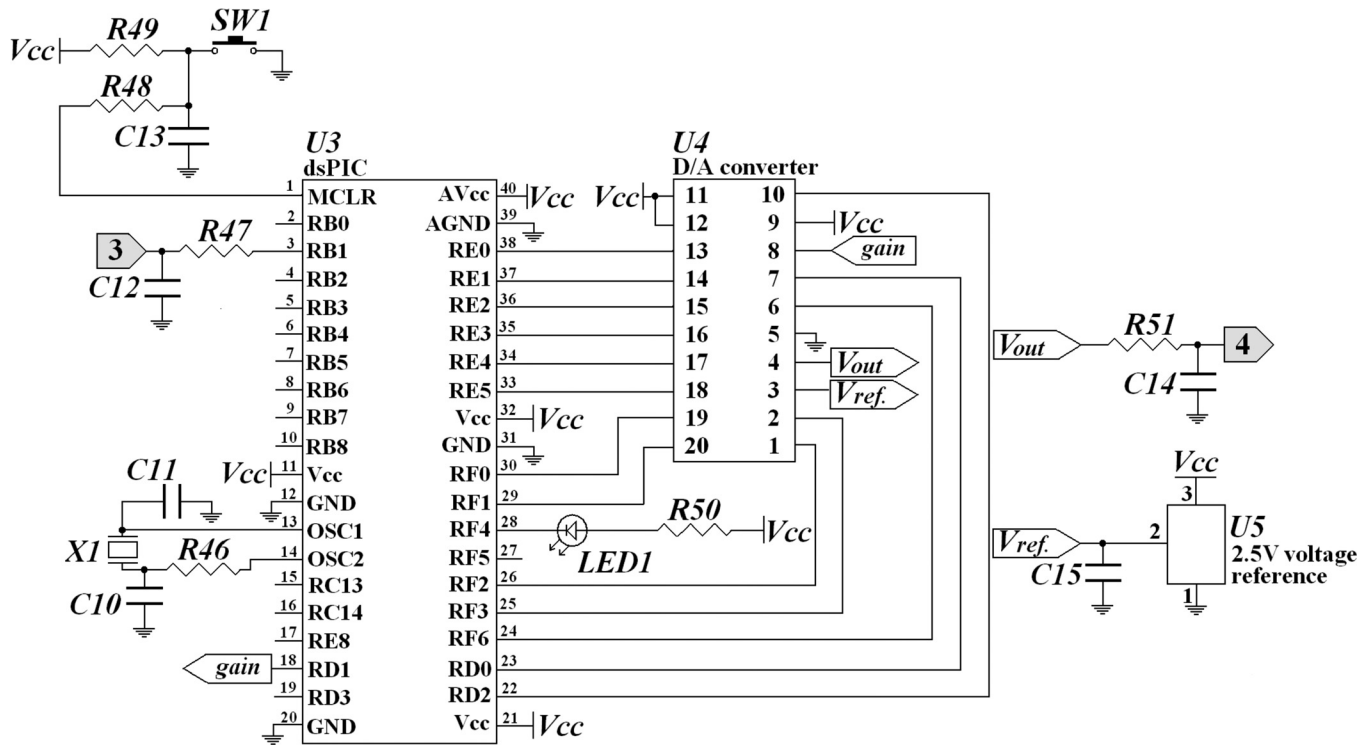


FIG. 5. The circuit diagram of the digital part in the analog-digital hybrid cell model.

the values of the ionic currents and the membrane potential in LR-I model were too small and difficult to handle on the scale of the analog circuits. In particular, we converted the scales as follows: 8 μA of LR-I to 3 mA of the hybrid cell model, -100 mV of LR-I to 0 V of the hybrid and 120 mV of LR-I to 5 V of the hybrid cell model. In formulae, the scale conversions of the voltage and the current are expressed as follows:

$$\frac{V_{LR-I}[\text{mV}] + 100}{220} \times 5 \rightarrow V_{\text{hybrid}}[\text{V}] \quad (4)$$

$$I_{LR-I}[\mu\text{A}] \times \left(\frac{3}{8}\right) \rightarrow I_{\text{hybrid}}[\text{mA}]$$

The action potential waveform for the single cell produced by the LR-I model is shown in Fig. 6(a) in order to compare with that produced by the hybrid cell model shown in Fig. 6(b) with the original voltage/current scales and in Fig. 6(c) with the converted scales. An impulsive stimulation with a duration of 1 ms and an intensity of 80 μA was applied to LR-I and also to the hybrid cell model, showing that the action potential waveform produced by the hybrid cell model was quantitatively the same as that by LR-I model. In particular, both models showed almost the same action potential duration (APD): about 350 ms. Moreover, it was confirmed that the dynamics of the hybrid cell model, in response to periodic current impulse trains with a variety of the period, reproduced the corresponding dynamics of the LR-I model well.⁵¹ See supplemental material to confirm the extent to which the I - V relationships of the hybrid cell model could reproduce those of the LR-I model.⁶⁶ Major differences observed at the period after

the initial rapid depolarization for about 100 ms were due to a variability of analog devices (mainly the operational amplifiers) and the I - V relationship of I_{Na} as discussed later in Sec. V.

III. REENTRANT ACTION POTENTIAL CONDUCTION IN ACTIVE CABLE MODELS

Propagation of action potentials in an excitable tissue is often modeled by a continuous excitable medium, leading to a model described by a reaction-diffusion equation. In particular, we consider a spatially one dimensional and homogeneous medium. Thus we have

$$\frac{\partial V_m(x, t)}{\partial t} = D \nabla^2 V_m(x, t) - \frac{I_{ion}(x, t)}{C_m} + \frac{I_{ext}(x, t)}{C_m}, \quad (5)$$

where $V_m(x, t)$ is the cardiac cellular membrane potential at position x and time t , ∇^2 is the second derivative with respect to the position x , $C_m = 1.0 \mu\text{F cm}^{-2}$ is the membrane capacitance, $D = (C_m S_v \rho)^{-1}$ is the diffusion coefficient, where S_v and ρ are the surface-to-volume ratio of the cardiac cells and the longitudinal tissue resistivity of cardiac muscle, respectively. According to the literature that use models of one and two dimensional cardiac tissues,^{26,52} we consider the case where $S_v = 5000 \text{ cm}^{-1}$ and $\rho = 0.2 \text{ k}\Omega\text{cm}$, leading to $D = 1 \text{ cm}^2 \text{ s}^{-1}$ which is $D = 10^{-3} \text{ cm}^2 \text{ ms}^{-1}$. $I_{ion}(x, t)$ is the ion channel current at position x and time t . Here, the I_{ion} is specified by the LR-I model. I_{ext} may also be position dependent if the externally applied current is spatially distributed. More specifically, we consider a one-dimensional ring of LR-I active cable as a model for exhibiting a circu-

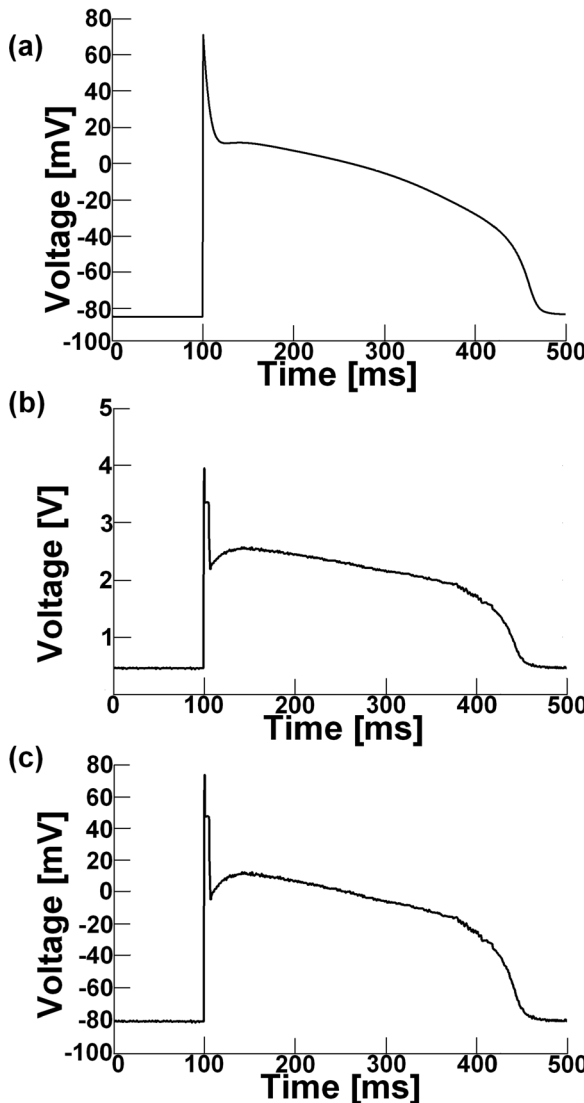


FIG. 6. Action potential waveforms of the LR-I and the hybrid cell model. Panels (a) and (b) represent the action potential waveforms generated by the LR-I model and the analog-digital hybrid cell model, respectively, in response to a single current pulse. Panel (c) shows the action potential waveform in the hybrid cell model after the scale conversion.

movement reentry, which is thought to be a typical mechanism of anatomical reentrant cardiac arrhythmia. Here, a ring of length $L=4.7$ cm is considered. Practically, this length was selected due to the number of hybrid cells available, and it might not be long enough for supporting a reentry excitation on the ring. This is because the typical conduction velocity of an action potential is about 60 cm/s in cardiac tissue,⁵³ resulting in a period of reentry about 78 ms for the ring. This reentry period is much smaller than a usual APD (about 150–200 ms) during conduction. In order to enable the ring to support a reentrant action potential, it was necessary to modify the dynamics of every single hybrid cell compartment so that the APD became smaller than usual. To this end, we modified the time scale of the I_{si} current dynamics of each cell for both LR-I and hybrid models. That is, the rate functions $\alpha_d(V_m)$, $\beta_d(V_m)$, $\alpha_f(V_m)$, $\beta_f(V_m)$ for the d and f gates of determining the I_{si} dynamics

for each of all LR-I and hybrid cell compartment models were doubled so that the time constant functions $\tau_d(V_m)$ and $\tau_f(V_m)$ were halved, resulting in a shorter APD in every single compartment. The modification could be performed easily for the hybrid cell models because the dynamics of I_{si} were implemented in each dsPIC used for each hybrid cell model. Although physiological situations corresponding to this modification is not necessarily obvious, we considered that it was not a problem for our purpose to examine whether the hybrid model could reproduce the corresponding LR-I dynamics.

The forward Euler spatial discretization with Δx for Eq. (5) gives the ordinary differential equation of the compartment model at position x of the LR-I cable as follows:

$$\begin{aligned} \frac{dV_m(x, t)}{dt} = & \frac{D}{(\Delta x)^2} (V_m(x + \Delta x, t) - V_m(x, t)) \\ & + \frac{D}{(\Delta x)^2} (V_m(x - \Delta x, t) - V_m(x, t)) \\ & - \frac{I_{ion}(x, t)}{C_m} + \frac{I_{ext}(x, t)}{C_m}. \end{aligned} \quad (6)$$

For numerical simulation of the LR-I cable, we segmented the ring into $N=80$ compartments, i.e., $\Delta x \simeq 0.058$ cm. This is equivalent with considering the gap junction resistivity between every adjacent compartments as $R_d=3.45$ k Ω cm². For the one-dimensional tissue cable, the compartment model with a set of ordinary differential equations can then be represented as

$$C_m \frac{dV_m^i}{dt} = \frac{1}{R_d} (V_m^{i+1} - V_m^i) + \frac{1}{R_d} (V_m^{i-1} - V_m^i) - I_{ion}^i + I_{ext}^i, \quad (7)$$

where $i=1, \dots, N=80$. V_m^i and I_{ion}^i are the membrane potential and the ion channel current of i th compartment, respectively. Note that $(i-1)$ refers to N for $i=1$ and $(i+1)$ refers to 1 for $i=N$, because of the ring geometry of the model. That is, the 1st and the N th compartments are connected by the gap junction of resistivity R_d . The non-ring shaped cable that has two open ends (referred to as the open-end cable) can also be established by disconnecting the 1st and the N th compartments, and it was used just for a comparison with the ring cable. This set of ordinary differential equations together with channel gating dynamics of every compartment for the LR-I were integrated numerically using the explicit Euler method with time step $\Delta t=0.001$ ms. With these parameters, the linear stability criterion $(\Delta x)^2/\Delta t > 4D$ is satisfied.

Although we tried to have quantitative reproduction of this LR-I cable model as much as possible using a ring-topology-network of 80 hybrid cell compartment models, it was required to modify the value of the gap junction resistance to $R_d=2.35$ k Ω cm², by which the conduction velocity of the action potential along the hybrid cable model became almost the same as that of the LR-I cable model as shown below.

Figure 7 shows non-conducting action potential waveforms of the single isolated cell models and conducting action potential waveforms of single cell compartment

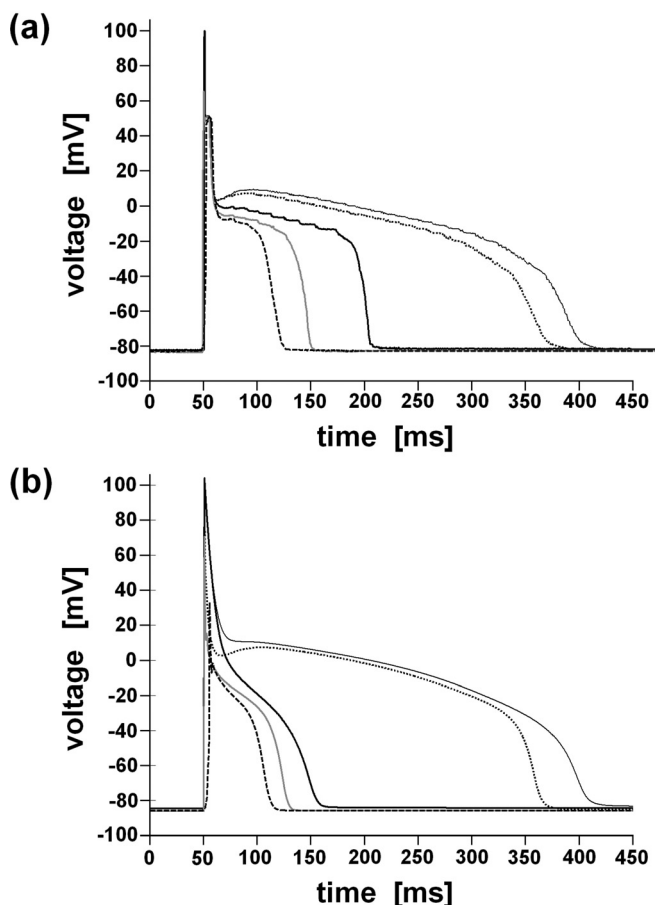


FIG. 7. Action potential waveforms of the hybrid cell model in (a) and LR-I model in (b). Thin solid curves: non-conducting action potentials in the single isolated cell with the original I_{si} dynamics. Dotted curves: conducting action potential along the open-end cable with the original I_{si} dynamics. Thick solid curves: non-conducting action potentials in the single isolated cell with the modified I_{si} dynamics. Gray curves: non-reentrant conducting action potential along the ring cable with the modified I_{si} dynamics. Dashed curves: reentrant action potential along the ring cable with the modified I_{si} dynamics.

models embedded in the open-end as well as the ring cables. In particular, it was examined how the APD was altered by the modification of the I_{si} dynamics and by the excitation conduction through the gap junction connection in the hybrid cell and the hybrid cable models as well as in the single LR-I and the LR-I cable models. In both Fig. 7(a) for the hybrid models and Fig. 7(b) for the LR-I models, the action potential with the largest APD of about 350 ms is from the single isolated cell models with the original I_{si} dynamics in response to a single current pulse stimulation applied to the cell model at the resting potential. The second largest APD of about 300 ms in each of the hybrid and LR-I models is from the conducting action potential along the open-end cable also in response to a sequence of current stimulations separated by a long time interval (1000 ms). The stimulations were applied at one end of the cable, and the action potential was recorded at the middle point of the cable during steady state dynamics of the periodically stimulated cable. The conduction velocity was about 35 cm/s for the open-end hybrid cable and about 31 cm/s for the open-end LR-I cable. The modification of I_{si} dynamics reduced APD in the single

isolated cell models as in the third largest APD of Fig. 7, where APD of the non-conducting action potential was about 150 ms for the single isolated hybrid cell model and about 100 ms for the single isolated LR-I. Differences in APD between the hybrid cell model and LR-I was due to a variability of analog devices and the $I-V$ relationship of I_{Na} (see discussion in Sec. V). Action potential conduction on the ring cable with the modified I_{si} dynamics reduced APD furthermore. In this case, APDs in the hybrid model and the LR-I model were about 100 ms and 80 ms, respectively, for non-reentrant conducting action potentials that were evoked by a sequence of long-time-separated current pulses applied at one point of the ring. The conduction velocity in this non-reentrant conduction was also about 35 cm/s for the hybrid ring cable and about 31 cm/s for the LR-I ring cable. APD was the shortest for the reentrant action potential with the modified I_{si} dynamics both in the hybrid ring and LR-I ring cables. It was about 70 ms in the hybrid ring cable and about 60 ms in the LR-I ring cable. The conduction velocity of the reentry was about 32 cm/s for the hybrid ring cable and about 28 cm/s for the LR-I ring cable. The reentrant conduction velocities obtained in the ring geometry were slower than those in the cable because the ring was effectively paced more rapidly, thereby invoking conduction velocity restitution. These conduction velocities during reentry are slower than the physiological conduction velocity,⁵³ but they are comparable to those obtained by some of previous studies.⁵⁴ In summary, the hybrid and the LR-I cables showed quantitatively similar characteristics in APD and conduction velocity for both with original and modified I_{si} dynamics, although we should discuss detailed differences between Figs. 7(a) and 7(b).

For the circus movement reentry to occur in the ring-shaped LR-I and the hybrid cable models with the modified I_{si} dynamics, an unidirectional block of conducting action potentials and the presence of an excitable gap are required where the excitable gap is defined as a spatial interval of the medium with enough excitability on the ring. Here, the unidirectional block was induced by using the so called S1-S2 protocol,^{12,54} in which single or several (usually equally time spaced) impulsive stimulations referred to as S1 were applied at a given location on the ring, and then another impulsive stimulation referred to as S2 was applied at a different location from the S1 site.

Panels (a) and (b) in Fig. 8 show space-time diagrams showing changes in the membrane potential as a function of time and position along the ring during initiation of reentry in the hybrid and LR-I cable models, respectively. See MPG video supplemental material⁶⁶ demonstrating the reentry dynamics observed in the hybrid circuit model. Quantitative reproduction of LR-I cable dynamics by the hybrid cable model can be confirmed. We used impulsive stimulations for S1 and S2 with a duration of 1 ms and an intensity of 150 μ A. In each figure, two S1 stimulations are applied to the ring at the compartment of number $i = 1$ (the bottom of the spatial axis in the panels), pacing the excitation of the medium. Each stimulus evokes excitation at the stimulated site, generating two conducting action potentials. One propagates clockwise and the other counter-clockwise along the ring. As is common

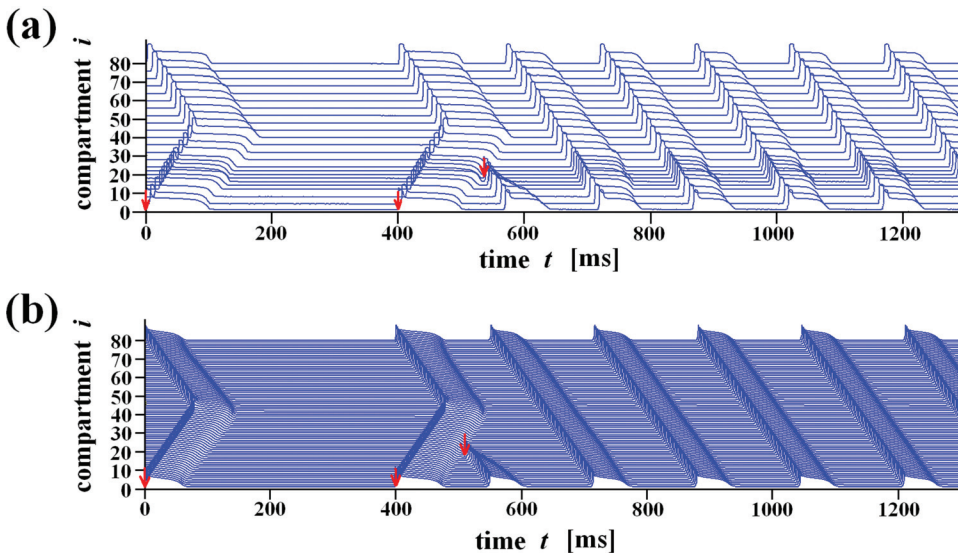


FIG. 8. (Color online) Space-time diagrams showing the membrane potential as a function of time and position around the ring tissue. (a) The analog-digital hybrid ring cable model. (b) LR-I ring cable model. In both models, I_{si} dynamics were modified to reduce APD so that the small ring could support the reentry. Arrow heads represent two S1 and single S2 stimulations. For the hybrid cable model, the membrane potentials were recorded only for the compartments 1, 4, 8, 12, 14, 16, 18, 20, 22, 24, 28, 32, 36, 40, 44, 48, 52, 56, 60, 64, 68, 72, 76, and 80, using a 24 ch recording device with analog-to-digital converters.

in excitable media, each conducting action potential possesses a wave-front and a tail. The wave-front progressively excites the compartments ahead of the wave-front, and the wave-tail is accompanied with refractoriness that decreases as it becomes distant from the action potential. These two conducting action potentials eventually collide with each other at the opposite side of the stimulated site, leading to annihilation of the action potentials due to the refractoriness located at each of the wave-tails. The S2, corresponding to an ectopic focus excitation in the real heart, is then applied at a position (the compartment number $i = 18$) slightly away from the S1 site at an appropriate time interval after the second application of S1. In order to initiate the reentrant wave, the S2 must be applied when the action potential generated by the S1 has passed through the S2 site and refractoriness of the wave-tail is still large in the one side of the S2 site (near side of the leaving action potential, referred to here as refractory side) but the excitability has regained on the other side referred to here as excitable side. The S2 with this specific timing generates an action potential that can propagate only to the excitable side (unidirectional block). Since the action potentials generated by the S1 are annihilated eventually, the single action potential generated by the S2 alone remains, initiating the circus movement reentrant wave.

The cycle length of the reentry in its steady state was $\bar{T}_{LR} = 165$ ms for the LR-I cable and that for the hybrid cable model was $\bar{T}_{hyb} = 149.3 \pm 1.6$ ms (mean \pm SD). The variability of the cycle length was only for the hybrid cable, and it was due to the random nature of the real circuit. As shown in Figs. 7 and 8, APD after the initiation of reentry was about 70 ms which was shorter than those generated in response to S1 stimulations in both the LR-I and hybrid cable models. This is because the wave-front of the reentrant wave is always chasing the wave-tail, and thus excitability of the ring cable cannot be fully recovered.

For delivering S1 and S2 stimulations to the hybrid cable model, we constructed an impulsive stimulator by using an H8/3694F microcontroller to control the timings of the stimulations systematically. See Appendix for details of

the circuit. Moreover, details of the electronic components and the source program written into the H8 microcontroller are described in the supplemental material.⁶⁶

IV. RESETTING AND ANNIHILATION OF REENTRY IN ACTIVE CABLE MODELS

Glass and his colleagues as well as other groups have been establishing a theory to handle this issue based on the phase resetting of nonlinear oscillators.^{55–62} Here, we utilize their theory for the LR-I and the hybrid ring cable models with modified I_{si} dynamics to show that the latter behaves satisfactorily as the former.

In the numerical and hardware experiments below, single and/or finite sequences of impulsive current stimulations were delivered to the ring cable models that support the reentry excitation as shown in the previous section. Those stimulations with the same stimulus intensity as in the unidirectional block experiment were applied again at the compartment of the number $i = 18$.

Panels (1a)-(1c) and (2a)-(2c) in Fig. 9 show space-time diagrams exemplifying the responses of the reentrant excitation to single stimulations as a function of time and position in the hybrid and LR-I ring cable models, respectively. One could observe a good coincidence between the dynamics of the hybrid and the LR-I ring cable models. In both Figs. 9(1a) and 9(2a), the stimulation was applied at the fully refractory side of the wave-tail of the reentry. Thus the stimulus failed to generate any propagating action potentials, less affecting the original reentry. In both Figs. 9(1b) and 9(2b), the stimulus was applied at a slightly later time instant than (1a) and (2a), generating a single action potential propagating only in a clockwise direction to collide with the originally counter-clockwise propagating action potential, leading to the annihilation of the reentry. This result suggests that a single stimulation delivered at an appropriate time interval referred to here as the annihilation interval, at which the wave-tail of the original reentry is located slightly away from the stimulation site, could annihilate the reentry. See MPG video

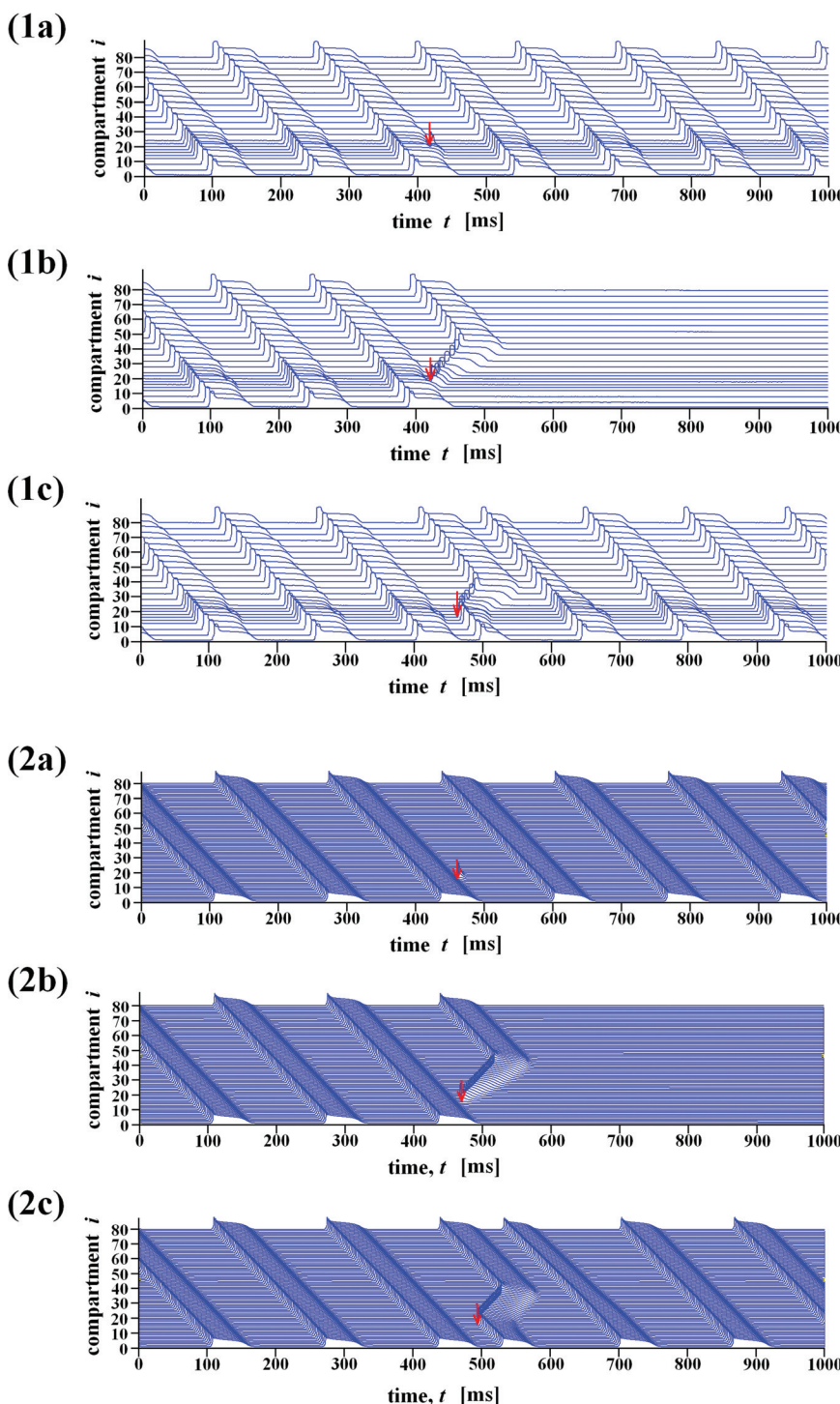


FIG. 9. (Color online) Responses of the reentry dynamics to single impulsive stimulations. (1a)-(1c) Responses of the hybrid ring cable model. (2a)-(2c) Responses of the LR-I ring cable model. In both models, I_{si} dynamics were modified as in Fig. 8. Each arrow head represents a stimulation.

supplemental material⁶⁶ demonstrating the annihilation of the reentry observed in the hybrid circuit model. In both Figs. 9(1c) and 9(2c), the stimulus was applied at the excitable gap located far behind the wave-tail of the original reentry, inducing two propagating action potentials in both clockwise and counterclockwise directions. The wave propagating in the clockwise direction collided with the original reentrant wave, and they were annihilated with each other. The wave traveling in the counterclockwise direction persisted, leading to the resetting of the reentrant circulation rhythm, where the successive occurrence times of excitation at every compartment

were advanced about 50 ms in comparison with the expected times for the original reentry excitation. These three cases are typical responses of the reentry.

The resetting (advance and delay of the circulation rhythm of the reentrant wave) and the annihilation of the reentry can be analyzed using the phase resetting curve (PRC) as performed in the previous studies^{55,56} in both hybrid and LR-I ring cable models. To this end, the phase of the reentrant wave is defined based on the time instant when the reentrant action potential is detected at a given recording site. Here, we located a recording site the same as the

stimulation site, i.e., the compartment number $i = 18$. First, the stimulation phase ϕ that takes a value between 0 and 1 is defined as

$$\phi = \frac{t_{stim}}{\bar{T}}, \quad (8)$$

where \bar{T} is the period of the steady state reentry with no stimulations, and t_{stim} is the time elapsed from the time instant when the last propagating reentrant action potential is detected at the recording site before the stimulation is applied. A small stimulation phase roughly between $0 < \phi < 0.45$, corresponding to roughly $0 < t_{stim} < 75$ ms, implies that the stimulation is applied when the stimulation site is in the middle of the reentrant action potential. A stimulation phase close to 1, corresponding to $t_{stim} \sim \bar{T}$, implies that the stimulation is applied close to an oncoming wave-front of the reentry excitation.

The amount of phase reset $\Delta\phi$ in response to a stimulation with its phase ϕ is defined as

$$\Delta\phi = \frac{\Delta T}{\bar{T}}, \quad (9)$$

where ΔT is the difference between the expected time instant of detecting the original reentrant action potential (when no stimulation is applied) and the time instant of detecting the reentrant action potential that is affected or newly generated by the stimulation. Positive and negative ΔT corresponds to phase delay and advance, respectively.

The result of detailed examinations on the responses of the reentry to stimulations delivered at various phases can be summarized using PRC. Figure 10 shows the PRC of the hybrid cable model (a) and that of the LR-I cable model. In both cases, the phase resetting was largely negative (advanced) when the stimulation phase is in the latter half of the reentry cycle. Only small amount of the phase resetting could be found for the stimulation phase between 0.1 and 0.45. When a stimulation is applied around the middle of the cycle length, roughly $0.47 < \phi < 0.56$ for the hybrid cable model and roughly $0.42 < \phi < 0.51$ for the LR-I cable model as depicted by vertical gray bands in Figs. 10(a) and 10(b), the reentry is annihilated by the stimulation as shown in Figs. 9(1b) and 9(2b). The phase interval corresponding to this gray band is referred to as the annihilation phase interval. Note that the PRC of the hybrid ring cable model in Fig. 10(a) was obtained by averaging three PRCs because the amount of resetting for a given stimulation phase could vary for every trial, possibly due to internal noises contaminated in the hardware circuits and small differences in the parameter values of every analog device. Moreover, for the hybrid cable model, the amount of phase reset at $\phi = 1$ was not exactly the same as that at $\phi = 0$. The difference was about 7 ms, and it was also due to the random fluctuation of the reentry period in the hybrid cable. Aside from this random nature in the hybrid model, the similarity between Figs. 10(a) and 10(b) is satisfactory.

Once we obtain the PRC representing the response of the reentrant wave to single stimulations at various stimu-

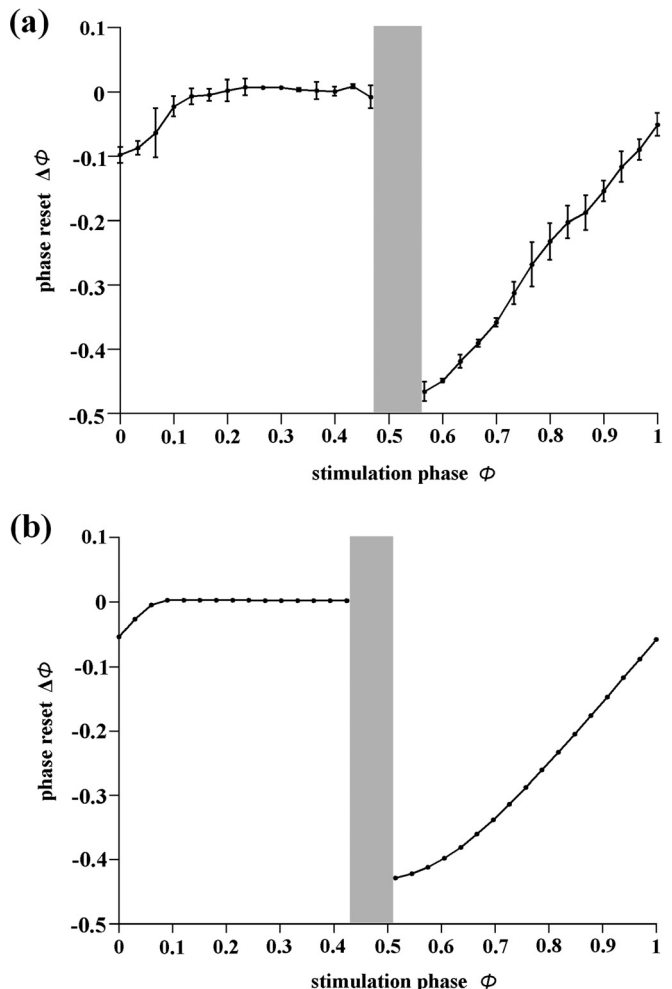


FIG. 10. The PRCs showing the amount of phase reset $\Delta\phi$ against the stimulation phase ϕ . (a) PRC of the hybrid ring cable model obtained by averaging three PRCs. Each error bar in (a) represents the standard deviation of the averaged three resetting values for three stimulations applied at the corresponding phase. (b) PRC of the LR-I ring cable model. Negative $\Delta\phi$ implies phase advance. The vertical gray band represents the annihilation phase interval. That is, the reentry is annihilated if a stimulation falls within this interval.

lation phases, we should be able to predict the dynamics of the reentry in response to a periodic sequence of the stimulations as examined in the previous study.⁵⁶ Let us consider the response of the reentry to a sequence of the stimulations with period T_{stim} . According to the theory of PRC, for a given phase of the first stimulation ϕ_1 , the second stimulation is applied at the phase $\phi_2 = \phi_1 - \Delta\phi_1 + T_{stim}/\bar{T} \pmod{1}$. In general, for a given n th stimulation phase, the $(n+1)$ th stimulation phase can be described as follows:

$$\phi_{n+1} = \phi_n - \Delta\phi_n + \frac{T_{stim}}{\bar{T}}, \pmod{1}. \quad (10)$$

Using this iterative mapping formulation, we can obtain a sequence of stimulation phases $\{\phi_n\}$ for a given initial stimulation phase ϕ_1 . If ϕ_n falls within the annihilation phase interval for the first time along the sequence, we can predict that the reentry is annihilated by the n th stimulation of the periodic train of the stimulations with period T_{stim} .

We examined whether this theory could predict the reentry dynamics in the hybrid cable model and the LR-I cable model. For each of these two cable models, we used the PRC obtained in Fig. 10 to establish the iterative mapping as in Eq. (10). As an example, we set $T_{stim} = 185$ ms and $\phi_1 = 0.6875$ for the hybrid cable model. Equation (10) with the PRC shown in Fig. 10(a) predicts that the first stimulation induces a relatively large delay $\Delta\phi_1 \sim -0.38$, followed by $\phi_2 = \phi_1 - \Delta\phi_1 + 1.25 \pmod{1} = 0.3193$, and $\phi_3 = \phi_2 - \Delta\phi_2 + 1.25 \pmod{1} = 0.5693$ which is within the annihilation interval. Figure 11 shows the dynamics of the hybrid ring cable model in response to this set of stimulations. The results confirm the prediction of the theory. That is, two stimulations separated by $T_{stim} = 185$ ms could not annihilate the reentry as in Fig. 11(1a), but three did as in Fig. 11(1b).

Another example performed for the LR-I ring cable used the stimulations with $T_{stim} = 200$ and $\phi_1 = 0.8182$. As in the hybrid cable model, Eq. (10) with the PRC of Fig. 10(b) for the LR-I cable predicts that $\phi_3 = 0.4732$ falls within the annihilation phase interval, and Figs. 11(2a) and 11(2b) confirmed this prediction. Quantitative similarity between Figs. 11(1a), 11(1b) and 11(2a), 11(2b) was satisfactory again, confirming a capability of reproducing the LR-I cable dynamics by the hybrid cable model. However, the similarity was not so much enough as we could predict LR-I dynamics using the PRC obtained from the phase resetting experiments in the hybrid cable model.

V. DISCUSSION

In this article, we showed that the proposed analog-digital hybrid circuit models of a single cell (hybrid cell model) and spatially distributed cable (hybrid cable model) were capable of reproducing action potential generation as well as the conduction of action potentials in the LR-I models of a cardiac ventricular cell and its one-dimensional cable. Good correspondence between the hybrid cable model and LR-I cable model was demonstrated using a one dimensional active cable as a model of anatomical reentry in a cardiac tissue with various conditions. Those include (1) unidirectional block to initiate reentry, (2) phase resetting by single impulsive stimulations, (3) annihilation of the reentry by appropriately timed single stimulations, (4) PRCs that can characterize the reentry dynamics in response to single stimulations at various timings, and (5) sequential phase resettings that leads to annihilation of the reentry as predicted by the one dimensional discrete Poincaré mappings.

Overall correspondence between the hybrid model and LR-I model was satisfactory. However, if we looked carefully at the action potential waveform in the single isolated hybrid cell model, it was different from one in the LR-I model for the interval right after the phase 0 upstroke as in Fig. 6. In particular, the initial phase 1 repolarization in the hybrid model was more pronounced. This was due to poor reproduction in the fast sodium current I_{Na} by the analog circuit. This is because I_{Na} is time-dependent with the time-dependent transient I-V relationship. As shown in the supplemental material,⁶⁶ the inward current response of the analog I_{Na} to the voltage clamp was smaller in amplitude and slower

in decay for most of the clamp voltages. As a possible handling, we tried to equalize net amount of the current inflow as much as possible. The small amplitude I_{Na} influx caused the pronounced repolarization at the phase 1. The poor reproduction of I_{Na} also induced the difference in the action potential waveform between the hybrid and LR-I models when we modified I_{si} dynamics as shown in Fig. 7, in which APD of the hybrid cell model was about 1.5 times longer than that of the LR-I model. This might be due to the slow decay of I_{Na} at the voltage around 0 mV. That is, the long lasting I_{Na} held back the repolarization even when I_{si} was decreased by the modification. A better reproduction of the transient I-V relationship for I_{Na} with other combinations of analog devices can improve agreement between the hybrid model and the LR-I model. Although we have tried to implement I_{Na} in the dsPIC, there was insufficient memory space in the dsPIC.

The hybrid cable model was able to perform real-time simulations of excitation propagation in cardiac tissues. It should be noted that, since each of single hybrid cell models always operates real-time and interact with neighboring hybrid cell models just through analog resistors, the real-time capability of the tissue circuit is completely independent of the number of the cell models and even topology of the connections between the cell models. In this study, we used a PC with Intel(R) Core(TM) 2 Quad CPU Q9550 2.83 GHz and 3.25 GB RAM. For the numerical simulation of LR-I cable with 80 compartments, it took about 20 s for 200 ms simulation time span that was roughly equal to one cycle length of the reentry. Of course it took just 200 ms for simulating 200 ms in the hybrid cable model. This is the meaning of the real-time capability in this study. That is, the hybrid model can interact electrically with real world cardiac cells if necessary. Although no optimization algorithms were introduced into the C or C++ source code program used for simulating the LR-I cable dynamics, the hybrid cable model was able to realize simulations over 100 times faster than those required for the numerical simulations of the LR-I cable model. Sophisticated techniques as well as HPC technology can speed the numerical simulation so that the speed ratio could be smaller than 100 obtained in this study. However, it will take a long time for numerical simulations of large scale cardiac tissues to catch up with real-time performance.

From the satisfactory correspondences that we examined here between the hybrid and LR-I cable models, and taking into account the real-time simulation capability of the hybrid model, we could conclude that the hybrid model might be a useful tool for large scale simulations of cardiac tissue dynamics, as an alternative to numerical simulations, leading toward further understanding of the reentrant mechanisms.

How can a cardiac tissue model with the hybrid cell models be large scale? Each analog-digital hybrid cell model used in this study was powered with ± 9 V, and the peak total current measured at the dc power sources $V+$ and $V-$ of Fig. 3 for the analog part of the model was 0.08 A and -0.06 A, respectively. For the digital part with 5 V dc power source (V_{CC}) of Fig. 5, it was 0.14 A. Simple calculations give us a rough estimation of the energy consumption in a single hybrid cell model, and it is about 2 W at most. For the hybrid cable model with N cell models, this becomes $2N$ W. The energy

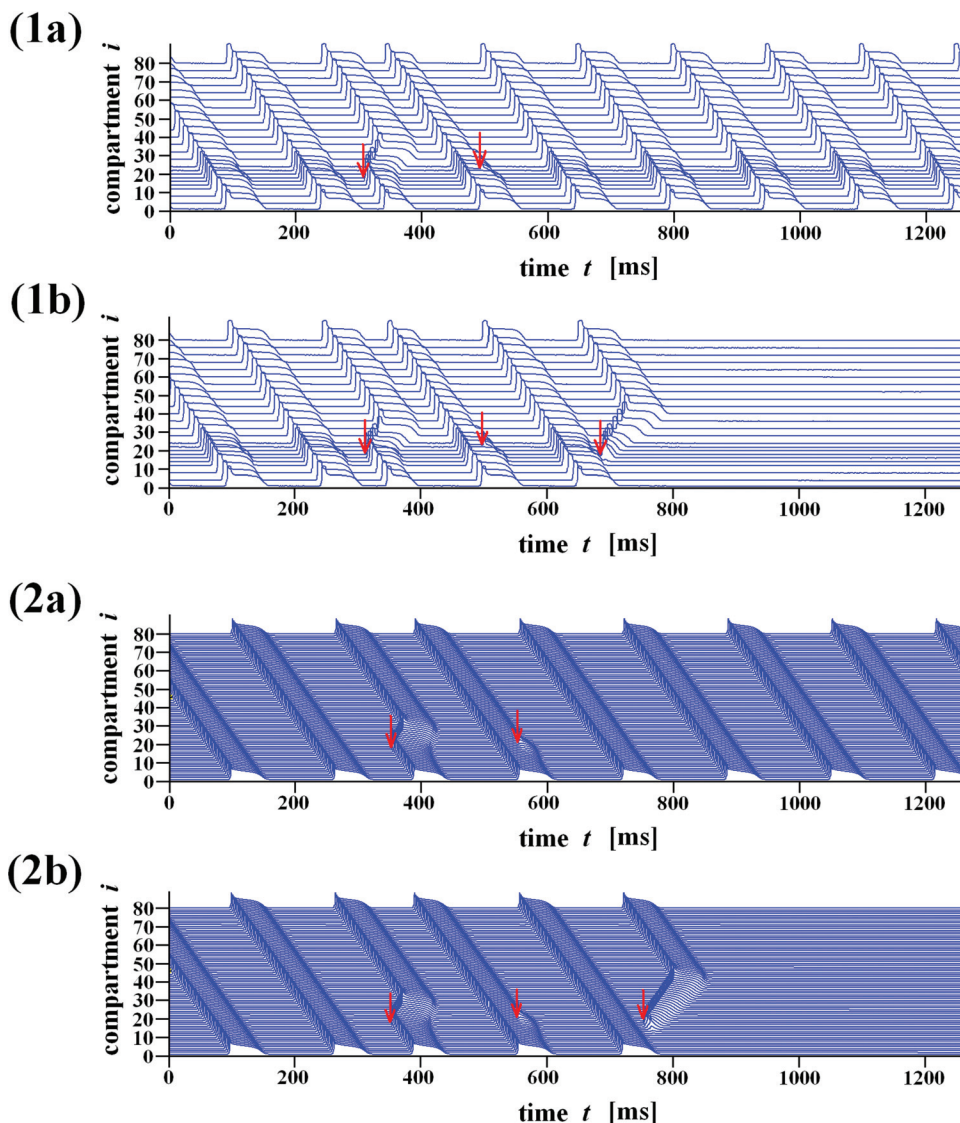


FIG. 11. (Color online) Sequential phase resettings that leads to annihilation of the reentry by a train of stimulations. (1a) and (1b) Reentry in the hybrid cable model was annihilated by three stimulations equally separated by $T_{stim} = 185$ ms in (1b) but not by two stimulations in (1a). (2a) and (2b) Reentry in the LR-I cable model was annihilated by three stimulations equally separated by $T_{stim} = 200$ ms in (2b) but not by two stimulations in (2a).

consumption of the hybrid cable model with $N=80$ is thus about 160 W, which is roughly comparable order with an energy consumption single desktop PC. This estimation implies that a large quantity of energy might be consumed for large scale real-time dynamics simulations. As the mission of the current study was to perform real-time simulations of excitation propagation, we were not concerned with the issue of minimizing the power consumption in the circuits. One way to achieve reduction in the energy consumption, and also reduction in the physical size of the circuit, is to implement this analog-digital hybrid circuit using LSI technology. Indeed, development of technology begins to allow for such realizations as attempted in some recent studies.^{63,64} Therefore, if the proposed hybrid cell model can be implemented as a LSI circuit in the future, dynamics of a large scale aggregation of the hybrid cell models as a cardiac tissue model can be simulated in real-time with a smaller energy consumption, where we would be able to address more complex dynamics of the heart tissue as a large scale excitable medium than the one exhibited by one dimensional tissue and control of them,

such as spiral wave propagations, break-up of spiral waves, and defibrillation of them.^{10,28,35,47,65}

ACKNOWLEDGMENTS

This work was supported in part by the Global COE program “*in silico* medicine” at Osaka University. The authors thank Toshihiro Shimizu, Takashi Sakuhana, and Takuji Nishimura for their help in developing prototypes of the hybrid circuit model.

APPENDIX: GLOSSARY OF CIRCUIT DIAGRAMS

Figure 12 shows nine circuit diagrams of the voltage sources (V1-V9) for generating the Nernst potentials and others of ion channel currents in the analog part shown in Fig. 4. Basically, general-purpose 6 V regulators (7806) are used to fix the voltage signal of V_+ to 6 V and capacitors are applied for smoothing the electrical signal. In some of the circuits, the voltage signal of 6 V is divided by voltage

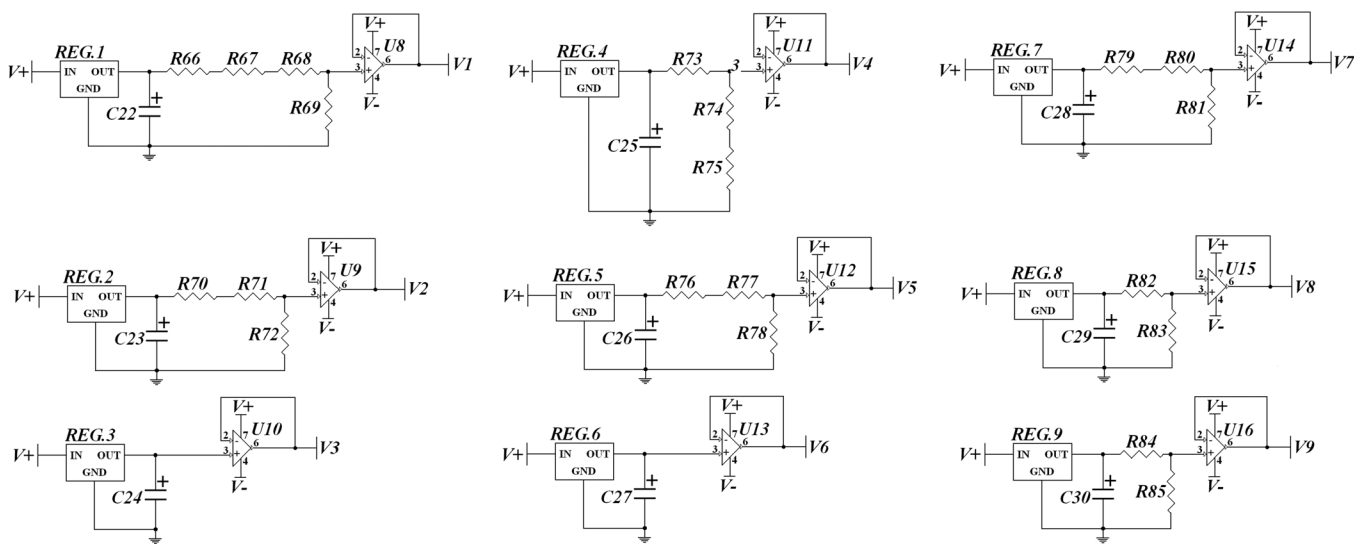


FIG. 12. Circuit diagrams of voltage sources in the analog part.

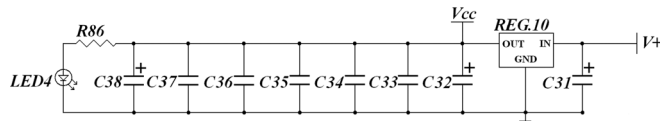


FIG. 13. A diagram of a power source circuit used in the digital part and the impulsive stimulator.

dividing circuits which consist of resistors as shown in the figure. Then, voltage followers which are constructed by using a general-purpose operational amplifier, LF356N, are applied to reinforce the current signal with the value of V_1 , V_2 , V_3 , V_4 , V_5 , V_6 , V_7 , V_8 , and V_9 as 1.3 V, 1.2 V, 6 V, 1.52 V, 2.3 V, 6 V, 1 V, 3 V, and 3.6 V, respectively.

Figure 13 shows the regulated +5 V (V_{CC}) dc power supply with 1 A current limiter for the dsPIC and the H8/3694F microcontroller. The base of this design is a general-purpose 5 V regulator (7805, REG.10) to maintain a constant voltage level at 5V and the capacitors for over-voltage protection and smoothing the electrical signal. The LED4 lights up whenever the power source is switched on. In this study, we used 9 V (V_+) and -9 V (V_-) supplied by a stabilized power source device.

Figure 14 shows the circuit of the impulsive stimulator for delivering current stimulations that induce and annihilate reentrant excitations. This circuit was powered by the same source that was used for the digital part of the hybrid cell model.

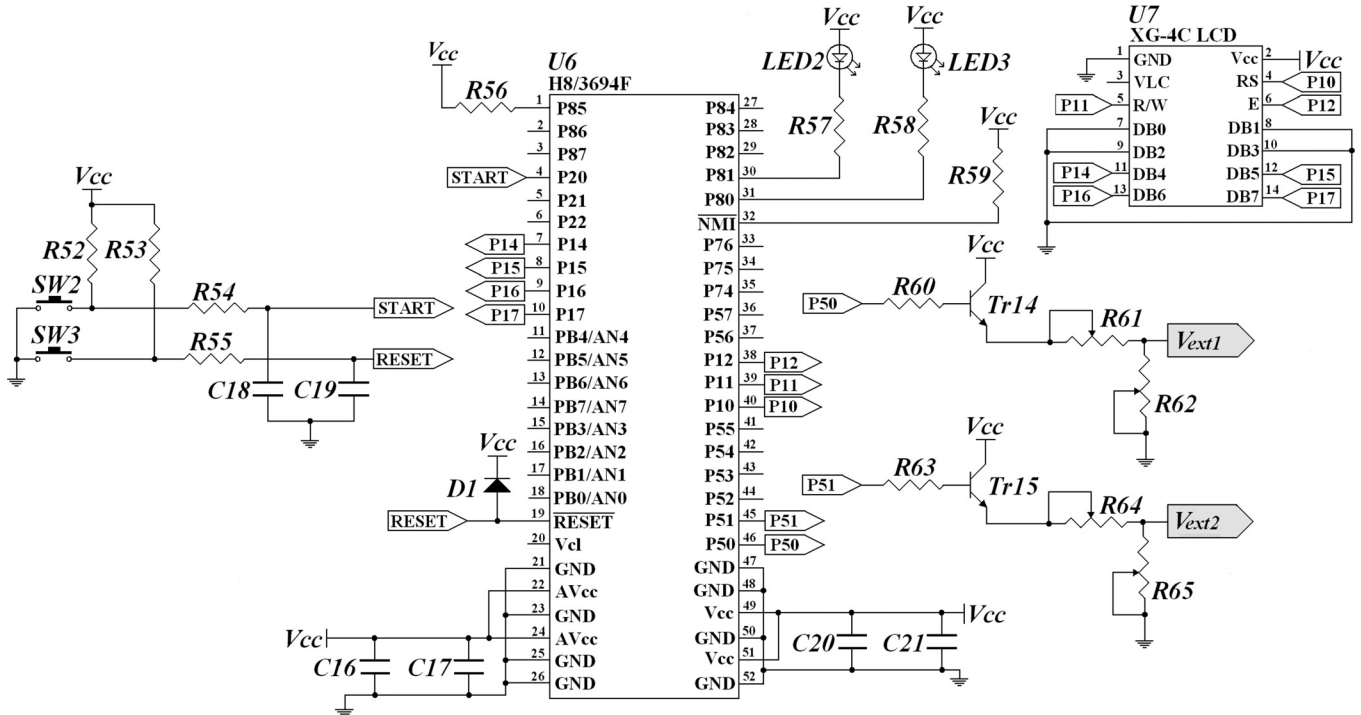


FIG. 14. The circuit diagram of the impulsive stimulator used to control timing of current injections to the hybrid cable model.

- ¹B. Hille, *Ion Channels of Excitable Membranes*, 3rd ed. (Sinauer Associates, 2001).
- ²Y. Rudy and J. Silva, *Q. Rev. Biophys.* **39**, 57 (2006).
- ³D. Kaplan and L. Glass, *Understanding Nonlinear Dynamics* (Springer-Verlag, 1995).
- ⁴R. Sasaki, Y. Watanabe, T. Morishita, and S. Yamagata, *Tohoku J. Exp. Med.* **95**, 177 (1968).
- ⁵G. Olivetti, M. Melissari, J. Capasso, and P. Anversa, *Circ. Res.* **68**, 1560 (1991).
- ⁶A. Winfree, *Science* **175**, 634 (1972).
- ⁷A. Winfree, *Chaos* **1**, 303 (1991).
- ⁸J. Davidenko, A. Pertsov, R. Salomonsz, W. Baxter, and J. Jalife, *Nature* **355**, 349 (1992).
- ⁹M. Markus, G. Kloss, and I. Kusch, *Nature* **371**, 402 (1994).
- ¹⁰M. Yamazaki, H. Honjo, H. Nakagawa, Y. Ishiguro, Y. Okuno, M. Amino, I. Sakuma, K. Kamiya, and I. Kodama, *Am. J. Physiol. Heart Circ. Physiol.* **292**, H539 (2007).
- ¹¹L. Tang, G. Hwang, H. Hayashi, J. Song, M. Ogawa, K. Kobayashi, B. Joung, H. Karagueuzian, P. Chen, and S. Lin, *Am. J. Physiol. Heart Circ. Physiol.* **295**, H297 (2008).
- ¹²M. Josephson and H. Wellens, eds., *Tachycardias: Mechanisms and Management* (Futura, Mount Kisco, NY, 1993), Vol. 6.
- ¹³A. L. Hodgkin and A. F. Huxley, *J. Physiol.* **117**, 500 (1952).
- ¹⁴R. Fitzhugh, *J. Gen. Physiol.* **43**, 867 (1960).
- ¹⁵D. Noble, *Nature* **188**, 495 (1960).
- ¹⁶G. W. Beeler and H. Reuter, *J. Physiol.* **268**, 177 (1977).
- ¹⁷C. Luo and Y. Rudy, *Circ. Res.* **68**, 1501 (1991).
- ¹⁸C. Luo and Y. Rudy, *Circ. Res.* **74**, 1097 (1994).
- ¹⁹C. Luo and Y. Rudy, *Circ. Res.* **74**, 1071 (1994).
- ²⁰D. Noble and Y. Rudy, *Philos. Trans. R. Soc. London, Ser. A* **359**, 1127 (2001).
- ²¹K. Ten Tusscher, D. Noble, P. J. Noble, and A. V. Panfilov, *Am. J. Physiol. Heart Circ. Physiol.* **286**, H1573 (2004).
- ²²M. Fink, S. Niederer, E. Cherry, F. Fenton, J. Koivumai, G. Seemann, R. Thul, H. Zhang, F. Sachse, D. Beard *et al.*, *Prog. Biophys. Mol. Biol.* **104**, 2 (2011).
- ²³R. Winslow, J. Rice, S. Jafri, E. Marban, and B. O'Rourke, *Circ. Res.* **84**, 571 (1999).
- ²⁴G. M. Faber, J. Silva, L. Livshitz, and Y. Rudy, *Biophys. J.* **92**, 1522 (2007).
- ²⁵J. Silva, H. Pan, D. Wu, A. Nekouzadeh, K. Decker, J. Cui, N. Baker, D. Sept, and Y. Rudy, *Proc. Natl. Acad. Sci. U.S.A.* **106**, 11102 (2009).
- ²⁶A. Xu and M. R. Guevara, *Chaos* **8**, 157 (1998).
- ²⁷D. Tran, M.-J. Yang, J. Weiss, A. Garfinkel, and Z. Qu, *Chaos* **17** (2007).
- ²⁸H. Henry and W.-J. Rappel, *Chaos* **14**, 172 (2004).
- ²⁹T. Ashihara, T. Namba, T. Ikeda, M. Ito, M. Kinoshita, and K. Nakazawa, *J. Cardiovasc. Electrophysiol.* **12**, 312 (2001).
- ³⁰K. Ten Tusscher and A. Panfilov, *Am. J. Physiol. Heart Circ. Physiol.* **291**, H1088 (2006).
- ³¹E. Cherry and F. Fenton, *Am. J. Physiol. Heart Circ. Physiol.* **292**, H43 (2007).
- ³²J. Alonso, J. Ferrero, V. Hernandez, G. Molto, M. Monserrat, and S. J., "Three-dimensional cardiac electrical activity simulation on cluster and grid platforms," in *High Performance Computing for Computational Science—VECPAR 2004, Lecture Notes in Computer Science*, edited by M. Dayde *et al.* (Springer-Verlag, Berlin, Germany, 2005), Vol. 3402.
- ³³S. Kharche, G. Seemann, L. Margetts, J. Leng, A. Holden, and H. Zhang, *Concurrency Comput.: Pract. Exper.* **20**, 1317 (2008).
- ³⁴F. Fenton and A. Karma, *Chaos* **8**, 20 (1998).
- ³⁵F. H. Fenton, E. M. Cherry, H. M. Hastings, and S. J. Evans, *Chaos* **12**, 852 (2002).
- ³⁶L. D. Harmon, *Kybernetik* **1**, 89 (1961).
- ³⁷J. Nagumo, S. Arimoto, and S. Yoshizawa, *Proc. IRE* **50**, 2061 (1962).
- ³⁸J. Nagumo, S. Yoshizawa, and S. Arimoto, *IEEE Trans. Circuit Theory* **12**, 400 (1965).
- ³⁹R. FitzHugh, *Biophys. J.* **1**, 445 (1961).
- ⁴⁰M. deCastro, E. Hofer, A. P. Munuzuri, M. Gomez-Gesteira, G. Plank, I. Schafferhofer, V. Perez-Munuzuri, and V. Perez-Villar, *Phys. Rev. E* **59**, 5962 (1999).
- ⁴¹N. Hoshimiya, S. Yoshida, K. Shogen, and T. Matsuo, *Biol. Cybern.* **35**, 125 (1979).
- ⁴²Y. Maeda and H. Makino, *BioSystems* **58**, 93 (2000).
- ⁴³Y. Maeda, E. Yagi, and H. Makino, *BioSystems* **79**, 125 (2005).
- ⁴⁴Y. Sekine, K. Torita, and J. Matsuoka, *Electron. Commun. Jpn., Part 2* **85**, 23 (2002).
- ⁴⁵K. Saeki, Y. Sekine, and K. Aihara, *Electron. Commun. Jpn., Part 2* **85**, 1 (2002).
- ⁴⁶G. Rachmuth and C.-S. Poon, *HFSP J.* **2**, 156 (2008).
- ⁴⁷F. Fenton, S. Evans, and H. Hastings, *Phys. Rev. Lett.* **83**, 3964 (1999).
- ⁴⁸R. Huffaker, S. Lamp, J. Weiss, and B. Kogan, *Heart Rhythm* **1**, 441 (2004).
- ⁴⁹K. Ten Tusscher and A. Panfilov, *Phys. Med. Biol.* **51**, 6141 (2006).
- ⁵⁰P. Schwartz, S. Priori, C. Spazzolini, A. Moss, G. M. Vincent, C. Napolitano, I. Denjoy, P. Guicheney, G. Breithardt, M. T. Keating, J. A. Towbin *et al.*, *Circulation* **103**, 89 (2001).
- ⁵¹F. Mahmud, T. Sakuhana, N. Shiozawa, and T. Nomura, *Trans. Jpn. Soc. Med. Biol. Eng.* **47**, 428 (2009).
- ⁵²M. Courtemanche, J. P. Keener, and L. Glass, *SIAM J. Appl. Math.* **56**, 119 (1996).
- ⁵³A. Kléber and Y. Rudy, *Physiol. Rev.* **84**, 431 (2004).
- ⁵⁴W. Quan and Y. Rudy, *Circ. Res.* **66**, 367 (1990).
- ⁵⁵L. Glass and M. Josephson, *Phys. Rev. Lett.* **75**, 2059 (1995).
- ⁵⁶T. Nomura and L. Glass, *Phys. Rev. E* **53**, 6353 (1996).
- ⁵⁷K. Hall and L. Glass, *Phys. Rev. Lett.* **82**, 5164 (1999).
- ⁵⁸Y. Nagai, H. González, A. Shrier, and L. Glass, *Phys. Rev. Lett.* **84**, 4248 (2000).
- ⁵⁹C. Ingelmo and L. Frame, *J. Cardiovasc. Electrophysiol.* **11**, 981 (2000).
- ⁶⁰L. Glass, Y. Nagai, K. Hall, M. Talajic, and S. Nattel, *Phys. Rev. E* **65**, 021908 (2002).
- ⁶¹C. Johnson and R. Barr, *J. Cardiovasc. Electrophysiol.* **14**, 1064 (2003).
- ⁶²T. Krogh-Madsen, L. Glass, E. Doedel, and M. Guevara, *J. Theor. Biol.* **230**, 499 (2004).
- ⁶³S. Kanoh, M. Imai, and N. Hoshimiya, *Syst. Comput. Jpn.* **36**, 84 (2005).
- ⁶⁴J. H. B. Wijekoon and P. Dudek, *Proceedings of International Joint Conference on Neural Networks, Orlando, FL*, 12–17 August 2007 (2007), pp. 1332–1337.
- ⁶⁵S. Sinha, A. Pande, and R. Pandit, *Phys. Rev. Lett.* **86**, 3678 (2001).
- ⁶⁶See supplementary material at <http://dx.doi.org/10.1063/1.3597645> for details of the circuit and MPG movies for hardware simulations performed on the hybrid model.